X-ray computed tomography supported by nuclear magnetic resonance and mercury porosimetry as novel approach in pore space characterization of tight sandstones

*Krakowska P., *Puskarczyk E., **Jędrychowski M., *Habrat M., ***Madejski P., ****Dohnalik M.
*AGH University of Science and Technology in Krakow (Poland), Faculty of Geology, Geophysics and Environmental Protection
**AGH University of Science and Technology in Krakow (Poland), Faculty of Physics and Applied Computer Science
***AGH University of Science and Technology in Krakow (Poland), Faculty of Mechanical Engineering and Robotics
****Oil and Gas Institute – National Research Institute (Poland)

This paper was prepared for presentation at the International Symposium of the Society of Core Analysts held in Trondheim, Norway, 27-30 August 2018

ABSTRACT

Tight, gas-bearing formations from Paleozoic basins in Poland were under careful analysis using nuclear magnetic resonance spectroscopy, NMR, mercury porosimetry, MICP, and computed X-ray tomography, CT. Results of laboratory measurements were used to calculate advance petrophysical parameters such as clay-bound, capillary-bound and moveable water for non-standard T2 distribution interpretation from NMR. Swanson parameter for fracture-porous systems were derived from MICP and sphericity and pore throat diameters from CT. Innovative approach in estimating pore throat diameter was introduced on the basis of best-fit ellipsoid radii. Moreover application of semivariogram for pores location allows assessing the heterogeneity in pore space structure as well as the qualitative interpretation of 3D objects (pores).

INTRODUCTION

Understanding the pore space development in tight gas-bearing formation remains a challenge. Unconventional tight gas porosity and permeability are quite difficult to interpret [1, 2, 3]. Pore space heterogeneity in tight sandstones can be determined using complementary data analysis from various laboratory methods [4]. Powerful nuclear magnetic resonance spectroscopy, mercury porosimetry and computed X-ray tomography provide answers about standard and advanced petrophysical parameters of rocks. However, computed X-ray tomography, besides the quantitative parameters, allows the 2D and 3D visualisation of pore space.

Methods and results of laboratory experiments are presented in the paper. Additionally, a combination of laboratory experiments is proposed in order to retrieve the information

about mutual relations between parameters. Two innovative approaches are presented: 1) pore throat diameter determination based on tomographic images parametrization and 2) semivariograms utility in heterogeneity analysis of pore space [5].

DATA SET AND METHOD

Research material consists of fifteen core samples from wells located in different geological units in Poland. Depths of cores present deposition is more than 3000 m. All samples are from tight, gas-bearing sandstones. Samples 1-7 are Cambrian, sample 8 – Ordovician, samples 9-12 – Devonian and samples 13-15 – Carboniferous. Granulometry provided information that all analysed samples are within sand grain size. Samples 11 and 12 were probed from the same Devonian tight sandstone formation but from different wells, whereas Cambrian samples 1-4 come from the same formation and well but different depths of present deposition.

NMR spectroscopy (NMR) was carried out using NMR Maran 23MHz (Oxford Resonance Instruments) with a permanent magnet generating a field of 0.56 T intensity [6]. All experiments were made at the temperature of 35 ^{o}C. All core samples (about 4 cm in length and 2.54 cm in diameter) were brine-saturated with 50 g/l or 250 g/l NaCl solutions depending on the sample location and age. The non-standard processing and interpretation of T2 distribution was conducted basing on fitting of selected functions – Gaussian or Weibull to measured signal in different parts of the signal. These parts of the signal were defined by user and differed from standard T2 cut-offs for clastic rocks – 3 and 33 ms (Table 1). The individual cut-offs were fitted on the basis of the division. Non-standard procedure gave more precise result in porosity, clay-bound water, capillary-bound water and moveable water values estimation [7, 8].

Mercury porosimetry (MICP) was made using porosimeter Micromeritics' AutoPore IV 9500. The maximum working pressure is 60,000 psi, while the minimal – less than the ambient pressure. Wide range of pressures gave the possibility to penetrate pores from the range of 0.003-300 μm. All samples were placed in core holder, which was filled with mercury in vacuum conditions. MICP data were used to calculate: effective porosity, dynamic porosity for gas, dynamic porosity for oil, percent of pores above 1 μm in diameter, percent of pores above 0.1 μm, average pore diameter, total pore area, Swanson parameter for the first porous system, second porous system and third porous system [9, 10].

Computed X-ray tomography (CT) was carried out using Nanotom S 180n General Electric Sensing & Inspection Technologies [11, 12]. Nanotom is equipped with a 57-W X-ray tube with maximum work voltage 180 kV. Hamamatsu 2300×2300 pixel 2D detector (Ham C 7942CA-02) records data with maximum spatial resolution about 600 nm. The reconstruction of CT images was provided by the Feldkamp algorithm for the cone-beam X-ray CT. The collected data was subjected to the 3D median filter.

Parameters dedicated to bones parametrization were calculated and tested in order to get the quantitative information about pore space structure from CT [13]. Bones, as porous material, are widely analyzed using CT measurements, hence several parameters, which are normally calculated in bones, were estimated for rock samples. Following parameters were estimated from CT images for objects (pores): volume of pores, x, y and z-coordinate of pore centroid, surface area, volume enclosed by surface mesh, moment of inertia around shortest principal axis, middle principal axis and longest principal axis, mean local thickness of pore, standard deviation of the mean local thickness, maximum local thickness, length of best-fit ellipsoid's long radius, intermediate radius and short radius and also Feret diameter; these parameters were used also to determine other parameters such as sphericity and pore throat diameter. Pore throat diameter was identified in the object by the very long radius of a best-fit ellipsoid. Studies were performed on different samples determined that objects can have a pore throat if their minor radius is lower than 25% of the major radius; we used this as requirement for pore throat recognition. Semivariograms in x, y and z-direction provided information about the heterogeneity in the orientation of pores throughout the whole sample. Moreover, semivariogram quantitatively assesses the spatial discontinuity of data. Pore regionalization, so the direction in pore location, can be recognized by analysing the increase of semivariance with increase of distance. This approach is proposed for pore space heterogeneity analysis. Qualitative interpretation of pore space development and quality-check of determined parameters, such as sphericity or pore throat diameter, were possible using new software poROSE for porous materials examination using images from CT [14].

RESULTS

Detailed results of data interpretation from different laboratory measurements are presented in Table 1 – results of nuclear magnetic resonance spectroscopy, Table 2 – results of mercury porosimetry and Tables 3 and 4 – results of computed X-ray tomography. Results of standard and non-standard interpretation of T2 distribution are shown in Table 1. The observed differences reflect the difference in values of clay-bound, capillary-bound and moveable water. Non-standard T2 cut-offs are presented in Table 1 and are the result of fitting the Gaussian or Weibull function to the measured signal. Obtained T2 cut-offs differ from standard ones – 3 and 33 ms for clastic rocks. NMR results using non-standard T2 cut-offs were in agreement with other laboratory results. Clay-bound water has higher values after application the non-standard interpretation of T2 distribution.

Table 2 shows the interpretation the mercury porosimetry data. Fracture-porous systems were detected in all samples. In some samples even three fracture-porous systems were visible; these are described by Swanson parameters. Effective porosity is very low in all samples, while pore diameter is quite variable. Obtained average pore diameters for all samples ranged from about 0.007 to 100 μm.

Parameters determined on the basis of computed X-ray tomography data are presented in Table 3. Sphericity of the pores (objects) was calculated using moment of inertia around shortest (I1) principal axis and around and longest (I3) principal axis (parameter Imin/Imax) and calculated on the basis of object enclosed volume and surface area (parameter sphericity). After supporting by qualitative interpretation in poROSE software it appeared that the sphericity parameter reflects better the sphere-shaped objects.

Pore size parameters were determined using different parameters: Thickness – sphere enclosed into the object and parameters called as major, intermediate and minor radius which described the length of the long, intermediate and short radius of the best-fit ellipsoid. Pore throat diameters were also estimated for objects which are built from pores and narrow pore throats.

Relation of average pore throat diameter and average pore diameter from logarithmic T2 mean from NMR is presented in **Fig. 1**. It is observed the increase of average pore throat diameter with decrease in average pore diameter from logarithmic T2 mean. Sample 8 (symbol: cross) did not follow the relationship. Moreover, relation of median of pore diameter from MICP and minimum value of best-fit ellipsoid major diameter is shown in **Fig. 2**. Three of the samples did not take part in the relation because most likely during the MICP experiments materials was additionally crushed after applying high pressures. It is assumption because MICP measurements was carried out on crushed material.

Fig. 3 shows very strong heterogeneity in pore space development in XY plane for all 15 samples. The X axis presents the distance increase between the pores centroids from CT data, while Y axis – semivariance function. However, pores are slightly regionalized in samples 1, 7, 13 and 14 but with lack of continuity (slight increase of variance with an increase of distance).

Quantitative analysis of parameters could not be creditable if it was not supported by qualitative interpretation. **Figs. 4-6** presents the 3D visualisation of pore space based on CT data in samples with different age. Almost all objects (pores) were separately analysed in regards to proper pore throat and sphericity estimation. Ordovician sample 8 (**Fig. 4**) is characterized by high amount of objects in the whole sample, while Devonian sample 11 – objects are concentrated in the upper part of XZ plane (**Fig. 5**). Carboniferous sample 13 (**Fig. 6**) revealed irregularity in pore space development in XZ plane. Summarizing, qualitative interpretation was essential in quality-check of estimated parameters and Semivariogram credibility.

CONCLUSIONS

Tight, gas-bearing formations from Paleozoic basins in Poland were characterized using nuclear magnetic resonance spectroscopy, mercury porosimetry and computed X-ray tomography very precisely. Parameters from CT normally used in bones parametrization were very useful in pore space evaluation.

Innovative approach in estimating pore throat diameter was introduced on the basis of best-fit ellipsoid radii to objects extracted from CT images. Application of semivariogram for pore locations allows assessing the heterogeneity in pore space structure. Sphericity determined based on enclosed volume and surface area appeared as a more reliable parameter compared to the pore roundness calculated from moments of inertia. Moreover, 3D visualization of CT data allows to find the best solution for selecting the parameter, which informs about the object roundness – sphericity or using moments of inertia and also check the credibility of semivariogram application in heterogeneity analysis of pore space.

ACKNOWLEDGEMENTS

This project is financed by the National Centre for Research and Development in Poland, programme LIDER, project no. LIDER/319/L–6/14/NCBR/2015.

REFERENCES

1. Kosakowski, P., Wróbel, M., Poprawa, P., "Hydrocarbon generation and expulsion modelling of the lower Paleozoic source rocks in the Polish part of the Baltic region", *Geological Quarterly*, (2010) **54**, 2, 241–256.
2. Kotarba, M .J., "Geology, ecology and petroleum of the lower Paleozoic strata in the Polish part of the Baltic region", *Geological Quarterly*, (2012) **54**, 2, 103-108.
3. Krakowska, P., Dohnalik, M., Jarzyna, J., Wawrzyniak-Guz, K., "Computed X-ray microtomography as the useful tool in petrophysics: a case study of tight carbonates Modryn formation from Poland", *Journal of Natural Gas Science and Engineering*, (2016) **31**, 67-75.
4. Jarzyna, J., Krakowska, P., Puskarczyk E., Wawrzyniak-Guz, K., Bielecki, J., Tkocz, K., Tarasiuk, J., Wroński, S., Dohnalik, M., "X-ray computed microtomography – a useful tool for petrophysical properties determination", *Computational Geosciences*, (2016) **20**, 5, 1155-1167.
5. Krakowska, P., Puskarczyk, E., Jędrychowski, M., Habrat, M., Madejski, P., Dohanlik, M., "Innovative characterization of tight sandstones from Paleozoic basins in Poland using X-ray computed tomography supported by nuclear magnetic resonance and mercury porosimetry", *Journal of Petroleum Science and Engineering*, (2018) **166**, 389-405.
6. Coates, G., Xiao, L., Prammer, M.G., "NMR logging. Principles and Applications", Halliburton Energy Services, Huston (1999).
7. Puskarczyk, E., "Assessment of Reservoir Properties of Rock through Nuclear Magnetic Resonance Phenomenon Application", Ph.D. Thesis, AGH UST Library, Krakow (2010).
8. Krakowska, P., Puskarczyk, E. "Tight Reservoir Properties Derived by Nuclear Magnetic Resonance, Mercury Porosimetry and Computed Microtomography

Laboratory Techniques. Case Study of Palaeozoic Clastic Rocks", *Acta Geophysica*, (2015) **63**, 3, 789–814.
9. Mao, Z.Q., Xiao, L., Wang, Z.N., Jin, Y., Liu, X.G., Xie, B., "Estimation of permeability by integrating nuclear magnetic resonance (NMR) logs with mercury injection capillary pressure (MICP) data in tight gas sands", *Applied Magnetic Resonance*, (2013) **44**, 4, 449–468.
10. Xiao, L., Liu, D., Wang, H., Li, J., Lu, J., Zou, Ch., "The applicability analysis of models for permeability prediction using mercury injection capillary pressure (MICP) data", *Journal of Petroleum Science and Engineering*, (2017) **156**, 589–593.
11. Cnudde, V., Boone, M., "High-resolution X-ray computed tomography in geosciences: A review of the current technology and applications", *Earth-Science Reviews*, (2013) **123**, 1-17.
12. Madonna, C., Quintal, B., Frehner, M., Almqvist, B.S.G., Tisato, N., Pistone, M., Marone, F., Saenger, E.H., "Synchrotron-based X-ray tomographic microscopy for rock microstructure investigations", *Geophysics*, (2013) **78**, 53–64.
13. Janc, K., Tarasiuk, J., Bonnet, A.S., Lipinski, P., "Semi-automated algorithm for cortical and trabecular bone separation from CT scans", *Computer Methods in Biomechanics & Biomechanical Engineering*, (2011) **14**, 1, 217–218.
14. Habrat, M., Krakowska, P., Puskarczyk, E., Jędrychowski, M., Madejski, P., "The concept of a computer system for interpretation of tight rocks using X-ray computed tomography results", *Studia Geotechnica et Mechanica*, (2017) **39**, 1, 101-107.

Table 1. Parameters determined on the basis of NMR. Symbols: φ NMR ind – total porosity based on individual cut-offs, φ eff NMR ind – effective porosity based on individual cut-offs, CBW ind – clay-bound water based on individual cut-offs, BVI in – capillary-bound water based on individual cut-offs, BVW in ¬ moveable water based on individual cut-offs, T2 cut-off 1 – T2 cut-off between CBW and BVI, T2 cut-off 2 – T2 cut-off between BVI and BVW, φ eff NMR std – effective porosity based on standard cut-offs, CBW std – clay-bound water based on standard cut-offs, BVI std – capillary-bound water based on standard cut-offs, BVW std ¬ moveable water based on standard cut-offs, T2ML – logarithmic T2 mean, AvAm – average amplitude of signal, r NMR av – average pore diameter from T2ML

No	ϕ NMR in	ϕ eff NMR in	CBW in	BVI in	BVW in	T2 cut-off 1	T2 cut-off 2	ϕ eff NMR std	CBW std	BVI std	BVW std	T2 ML	Av Am	r NMR av
	%	%	%	%	%	µs	µs	%	%	%	%	µs	a.u.	um
1	0.46	0.33	0.13	0.24	0.09	3398	23714	0.34	0.13	0.29	0.05	7752	383	0.36
2	1.07	0.58	0.49	0.53	0.05	6494	50478	0.76	0.31	0.66	0.1	7122	862	0.33
3	3.96	2.3	1.66	1.81	0.49	6494	50478	2.91	1.05	2.22	0.69	8603	3266	0.4
4	2.1	0.89	1.21	0.86	0.03	21286	119702	1.68	0.42	1.21	0.47	12038	1793	0.55
5	5.68	2.87	2.81	2.74	0.13	4677	16982	3.82	1.86	3.56	0.26	5658	82	0.26
6	2.31	1.09	1.23	0.78	0.31	13804	87096	1.36	0.95	0.91	0.45	6623	71	0.3
7	8.22	3.43	4.79	2.63	0.81	7244	69183	4.93	3.29	3.98	0.95	5863	276	0.27
8	4.82	3.74	1.08	2.73	1.02	4677	107152	3.98	0.84	2.22	1.76	17894	139	0.82

9	1.6	0.38	1.22	0.28	0.1	5888	23988	0.42	1.18	0.24	0.18	1994	44	0.09
10														
11	4.82	0.91	3.91	0.76	0.15	16982	45709	1.61	3.21	1.42	0.19	2185	101	0.1
12	0.38	0.07	0.31	0.05	0.02	5234	36517	0.08	0.31	0.05	0.03	1405	46	0.06
13	1.76	0.46	1.3	0.36	0.11	2754	40738	0.64	1.12	0.49	0.15	2305	39	0.11
14	0.8	0.16	0.65	0.12	0.03	5248	36308	0.18	0.62	0.15	0.03	1389	48	0.06
15	1.06	0.3	0.76	0.28	0.03	1445	4677	0.32	0.74	0.28	0.04	1989	33	0.09

Table 2. Parameters determined on the basis of MICP. Symbols: φ MICP – effective porosity, φ gas MICP – dynamic porosity for gas, φ oil MICP – dynamic porosity for oil, Pores>1 μm – percent of pores above 1 μm in diameter, Pores>0.1 μm – percent of pores above 0.1 μm in diameter, d MICP – average pore diameter, TPA – total pore area, S1 – Swanson parameter for the first porous system, S2 – Swanson parameter for the second porous system, S3 – Swanson parameter for the third porous system

No	ϕ MICP	ϕ gas MICP	ϕ oil MICP	Pores>0.1 μm	Pores>1 μm	d MICP	TPA	S1	S2	S3
	%	%	%	%	%	μm	m2/g	frac/ psia	frac/ psia	frac/ psia
1	1.8	1.34	1.09	74.32	60.81	0.11	0.69	4.48E-04	8.98E-06	
2	4.63	3.26	1.65	70.39	35.53	0.11	0.26	2.95E-04	5.83E-06	
3	1.71	1.3	0.7	76.47	41.18	0.18	0.35	1.73E-04	3.73E-06	
4	4.45	3.7	1.47	83.16	33.16	0.18	0.15	1.72E-03	1.65E-05	
5	0.74	0.34	0.14	46.31	19.21	0.07	1.23	1.88E-04	8.73E-06	2.37E-06
6	0.29	0.28	0.17	97.26	57.53	0.66	0.04	4.72E-04	2.55E-05	7.33E-06
7	1.21	0.66	0.21	54.35	17.08	0.07	1.96	1.96E-04	2.03E-05	
8	0.82	0.67	0.22	81.68	26.7	0.1	0.78	2.98E-04	2.02E-05	3.60E-06
9	0.1	0.09	0.09	92.31	88.46	2.66	0	1.29E-04	4.11E-05	2.60E-06
10	0.03	0.04	0.04	100	100	50.02	0	5.82E-05	5.00E-08	
11	0.79	0.54	0.19	68.54	24.16	0.09	0.79	1.67E-04	1.64E-05	1.68E-06
12	0.17	0.11	0.11	66.67	64.44	0.05	0.38	4.37E-04	6.13E-07	
13	0.23	0.11	0.1	47.54	44.26	0.06	0.4	1.27E-04	1.23E-06	
14	4.44	4.18	3.88	94.31	87.39	0.39	0.83	7.93E-03	9.70E-05	5.49E-06
15	0.09	0.07	0.06	81.48	62.96	0.04	0.25	2.89E-14	5.31E-05	1.35E-07

Table 3. Parameters determined on the basis of CT. Symbols: φ CT – total porosity, Volume – volume of pore (object), I1 – moment of inertia around shortest principal axis, I2 –around middle principal axis, I3 – around longest principal axis, Imin/Imax – parameter describing sphericity of the object, Sphericity – sphericity calculated on the basis of enclosed volume and surface area, Av – average value, St.Dev. – standard deviation

No	ϕ CT	Volume	Surface Area	Enclosed Volume	I1	I2	I3	Imin/Imax	Sphericity
	%	μm^3	μm^2	μm^3	unitless	unitless	unitless	unitless	unitless

		Av	St.Dev.	Av	St.Dev.	Av	St.Dev.	Av	St.Dev.	Av	St.Dev.	Av	St.Dev.	Av	St.Dev.	Av	St.Dev.
1	0.05	152	1079	27	100	21	144	2.61E+05	6.12E+06	2.39E+05	5.56E+06	5.35E+04	1.05E+06	0.57	0.19	0.86	0.08
2	4.1	6934	50168	490	2312	992	6705	1.33E+08	3.25E+09	1.16E+08	2.83E+09	4.10E+07	1.16E+09	0.42	0.18	0.76	0.11
3		-	-	-	-	-	-	-	-	-	-	-	-	-	-	-	-
4	1.7	970	8097	111	708	123	1022	1.79E+07	1.24E+09	1.09E+07	7.02E+08	7.32E+06	5.44E+08	0.46	0.18	0.83	0.1
5	3.1	3094	13455	277	906	396	1702	6.13E+06	8.50E+07	5.27E+06	7.36E+07	2.16E+06	3.06E+07	0.5	0.21	0.83	0.12
6	2.3	8797	50756	600	2804	1143	6455	1.25E+08	4.51E+09	1.08E+08	4.06E+09	3.59E+07	1.01E+09	0.49	0.23	0.81	0.13
7	0.1	363	4199	47	253	51	573	6.33E+05	2.44E+07	5.59E+05	2.19E+07	1.15E+05	3.63E+06	0.6	0.19	0.86	0.08
8	3.94	253	723	62	102	17	35	4.23E+05	3.12E+07	3.62E+05	3.09E+07	6.17E+04	7.28E+05	0.3	0.14	0.52	0.09
9		-	-	-	-	-	-	-	-	-	-	-	-	-	-	-	-
10	0.07	442	1502	62	139	60	197	1.41E+05	1.77E+06	1.20E+05	1.52E+06	3.85E+04	4.25E+05	0.57	0.2	0.86	0.08
11	2.3	6030	51134	387	2242	806	6619	4.42E+07	1.02E+09	3.72E+07	8.41E+08	1.60E+07	4.09E+08	0.52	0.2	0.84	0.11
12		-	-	-	-	-	-	-	-	-	-	-	-	-	-	-	-
13	0.37	1432	20315	143	1561	190	2634	3.19E+07	1.97E+09	2.43E+07	1.45E+09	8.13E+06	5.45E+08	0.54	0.2	0.85	0.1
14	0.21	714	6631	77	490	97	873	2.04E+06	1.21E+08	1.52E+06	8.53E+07	6.79E+05	3.87E+07	0.58	0.19	0.86	0.09
15	0.11	444	1747	63	155	59	228	1.53E+05	1.94E+06	1.31E+05	1.69E+06	4.43E+04	5.15E+05	0.54	0.2	0.84	0.09

Table 4. Pore size parameters (in μm) from CT data

	Thickness		Maximum Thickness		Major diameter		Intermediate diameter		Minor diameter		Feret diameter		Pore throat diameter	
No	Av	St. Dev.	Av	St. Dev.	Av	St. Dev.	Av	St. Dev.	Av	St. Dev.	Av	St. Dev.	Av	St. Dev.
1	2.67	1.71	2.79	1.95	135.89	1203.32	423.91	3161.78	386.88	6546.45	3.15	3.77	15.96	11.07
2	4.93	4.36	5.77	5.61	140.93	837.59	538.02	11161.84	100.89	698.40	12.98	19.44	20.45	44.33
3	-	-	-	-	-	-	-	-	-	-	-	-	-	-
4	4.37	2.77	4.85	3.43	137.71	3468.99	178.52	3100.54	67.61	476.78	6.81	8.15	20.43	87.50
5	6.79	3.43	7.50	4.34	78.12	708.34	151.99	1949.01	70.30	887.96	9.99	11.74	16.30	38.41
6	7.41	4.29	8.44	5.77	60.12	655.80	111.52	935.27	127.40	2738.23	13.78	20.92	13.63	15.56
7	3.94	2.47	4.05	2.66	546.70	5112.02	1414.26	21312.22	245.20	1709.89	3.97	4.66	40.96	33.10
8	1.60	0.01	1.61	0.14	1367.74	12815.85	1365.69	11090.57	1177.03	40509.60	9.54	12.70	59.38	169.00
9	-	-	-	-	-	-	-	-	-	-	-	-	-	-
10	4.34	2.61	4.52	2.88	195.33	947.72	489.82	2618.50	178.34	831.19	5.01	5.40	31.57	44.03
11	7.28	4.59	8.00	5.67	362.83	6821.79	222.21	1695.26	128.96	1503.11	11.16	14.99	33.19	64.06
12	-	-	-	-	-	-	-	-	-	-	-	-	-	-
13	5.16	2.95	5.50	3.42	215.67	2211.39	1056.20	28177.11	224.20	2218.41	6.75	10.23	28.24	26.95
14	4.51	2.79	4.71	3.16	298.12	2360.74	710.45	10387.77	683.73	25588.44	4.98	6.47	48.45	55.55
15	4.22	2.42	4.46	2.80	3937.34	163526.99	2934.34	120380.41	296.02	4896.35	5.13	5.46	70.66	257.82

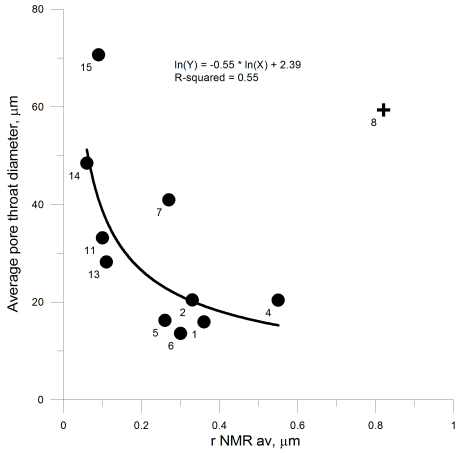

Fig. 1. Relation of average pore throat diameter from CT and average pore diameter from logarithmic T2 mean from NMR

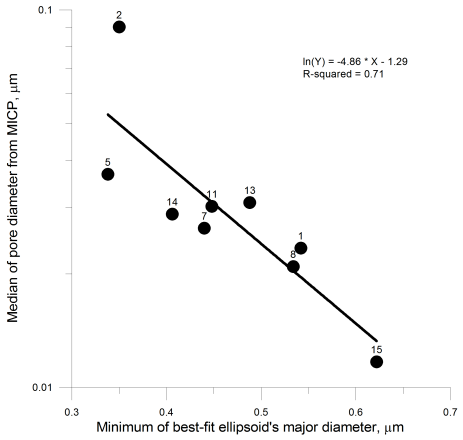

Fig. 2. Relation of median of pore diameter from MICP and minimum value of best-fit ellipsoid major diameter from CT

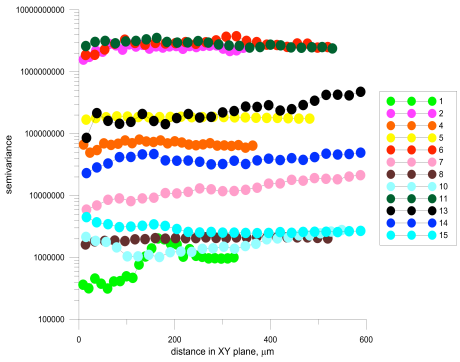

Fig. 3. Semivariogram of pores centroid coordinates, XY plane for all 15 samples

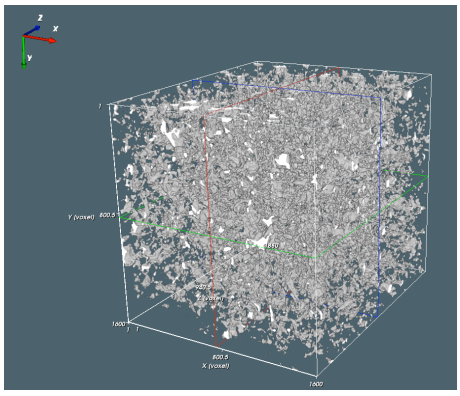

Fig. 4. 3D visualization of pore space from CT data, Ordovician sample 8

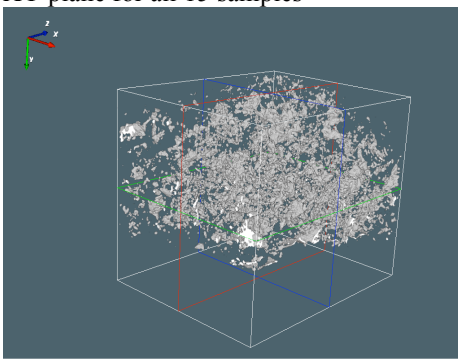

Fig. 5. 3D visualization of pore space from CT data, Devonian sample 11

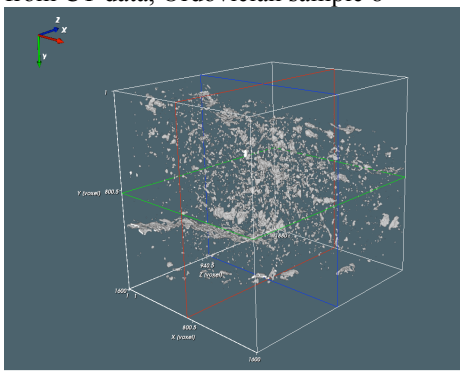

Fig. 6. 3D visualization of pore space from CT data, Carboniferous sample 13